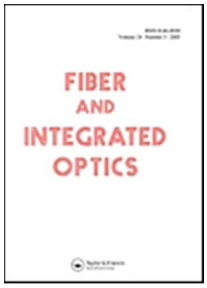

Control Strategy of True Time Delay Lines

Journal:	*Fiber and Integrated Optics*
Manuscript ID	UFIO-2016-2039.R1
Manuscript Type:	Special Issue: RF Photonics
Keywords:	All-Optical Signal Processing, radio over fiber, ring resonator

Control Strategy of True Time Delay Lines

Sebastian Rabal,[a] Laureano A. Bulus Rossini,[b] Pablo A. Costanzo Caso,[b,*]
[a]Centro de Investigaciones Ópticas (CONICET CCT La Plata, CIC Pcia. Bs. As., Universidad Nacional de La Plata). Camino Centenario y 508, La Plata 1900, Argentina.
[b]Instituto Balseiro (CNEA, Universidad Nacional de Cuyo) Av. Bustillo 9500, Bariloche 8400, Argentina.

Abstract. This paper presents the control of adjustable true time delays applied to an optical beamforming system. First is introduced the response of ring resonators of two and four ports and the cascade and lattice structures. The coupling factor and the phase modulation are employed as the control parameters for the adjustable group delay. The strategy of control is proposed and applied to a cascade of five ring resonator for producing wideband true time delays in the ps-ns range with 2 GHz bandwidth and extremely low ripple. Ripples lower than 0.1% were obtained for the adjusted group delays. The proposed strategy can simply be extended if more resonators are added to increase the bandwidth of the system.

Keywords: True time delay, optical delay line, ring resonator, beamforming, control strategy.

*Corresponding Author: E-mail: pcostanzo@ib.edu.ar

1 Introduction

Optical ring resonators (ORR) are devices extensively investigated due to its attractive features that make them suitable for a variety of applications in the field of photonic signal processing, among which may be mentioned the implementation of tunable filters, photonic sensors, optical delays, laser resonators, add-drop multiplexers for WDM (Wavelength Division Multiplexing) channels, dispersion compensators, and more. Initially, these devices were fabricated using optical fibers, and their dimensions and construction characteristics conferred them certain properties that made them suitable for some applications [1-7]. Nowadays, with the advancement of technology and manufacturing techniques, it is possible to build integrated devices with improved characteristics [8,9]. Also, in recent years have been studied various topologies and configurations of resonator devices with promising characteristics in the field of photonic signal processing [10,11].

An interesting application of ORRs is the implementation of optical delay lines for optical beamformer (OBF) systems [12-14], due to the inherent advantages of photonic devices for

microwaves signal processing, such as reduced weight and size of the system, wide bandwidth, low and constant attenuation over a wide frequency range, immunity to electromagnetic interference and low dispersion. But perhaps the most motivating of the advantages, by considering their electronic counterparts, is the independence with the frequency of the produced time delays. This characteristic solves the drawback known as beam squint where the microwaves signals of different frequencies are irradiated with different angles. In a previous work the operation and characteristics of adjustable ORRs were analyzed and a cascade of rings was proposed in order to increase the bandwidth of the OBF system [15]. To accomplish the implementation, it is required to calculate the values of the coupling factors and the phase shifts for each ring, in order to achieve a flat response in a given bandwidth.

Control strategies of delay lines have an important role for the proper functioning of a beamforming system, and are as important as the design of the delay lines itself. Currently, there are control systems based on the switching of binary optical delay lines, which exponentially increases its complexity when great resolution is required because many switches are necessary [16,17]. On the other hand, control strategies for delay lines implemented with FBG mounted on mechanical pieces, which deforms and modify the reflection pattern of the grating, were developed [18]. These solutions while offering continuous delay variation turn out to be little robust for some applications. Another control strategy is based on controlling the swept of the wavelength of a tunable laser [19]. Based on integrated ORRs different structures were implemented where many parameters can be controlled in order to obtain the required group delay [13]. These structures have complicated responses and, to our knowledge, a detailed analysis to implement a control strategy to produce broad band delay lines with reduced ripple,

has not been done so far. In this paper we propose a new scheme to continuously control de delay lines based on the cascade of ORRs.

The paper is structured in the following manner: Section 2 introduces the basic theory and models of single ORR with two and four ports, where the main parameters and how they modify the response of the device are presented. Then more complex structure are analyzed where cascade and lattice configurations were investigated. In Sec. 4 a practical strategy to control the response of a delay line composed of five cascaded ORRs is presented. The numerical simulation and results are discussed in Sec. 5, where a practical application is presented. It will be show the attractive features of the method such as the simplicity of the implementation and the information that can be obtained from the generated delays. Finally, in Sec. 6, the paper is concluded with a brief summary of the work and the most relevant results.

2 Theoretical Background

2.1 Operation and Modeling

ORR consists of two waveguides, one of them with a straight shape and the other one with a ring shape. Both are located very close together so that their evanescent fields overlap. In this way, part of the light propagating through the straight guide is coupled to the ring, which under certain conditions behaves as an optical resonant cavity. Fig. 1(a) shows a scheme of the device, where the amplitude of the electric field at each arm $i = 1\ldots4$, E_i, the coupling factor, k, and the phase modulation, ϕ, are presented.

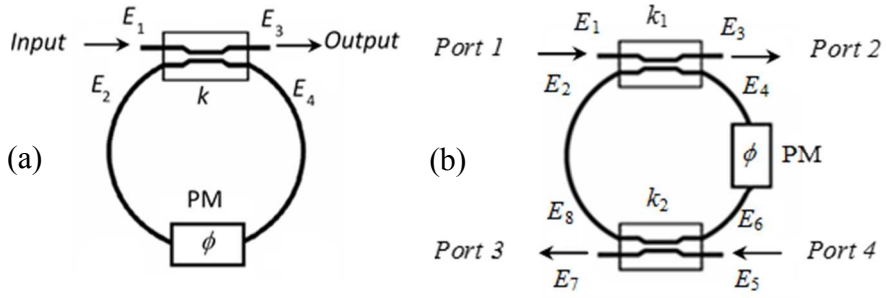

Fig. 1 Scheme of tunable two-port ORR (a), and four-port ORR (b). PM: Phase modulation.

If λ is the wavelength of light in vacuum, n_{ef} the effective index of refraction of the guide and L is the length of the ring, the resonance condition can be expressed as $\theta = 2\pi L n_{ef}/\lambda = 2\pi N$, and solving for L results $L = \lambda N/n_{ef}$, where $N \in \mathbb{Z}$. It can be observed that this condition is satisfied when L is an integer multiple of the propagating wavelength.

A mathematical model that describes the operation of the device was obtained in previous works [1,14] and we rewrite the transfer function in steady state condition that relates the electric fields at the input and output ports, E_3 and E_1, which is given by:

$$t_{31}(\Omega) = \frac{E_3}{E_1} = \frac{\xi\sqrt{1-k} - \xi^2\sqrt{a}\exp(-j\phi)\exp(-j\Omega)}{1-\xi\sqrt{1-k}\sqrt{a}\exp(-j\phi)\exp(-j\Omega)}, \quad (1)$$

where $a = \exp(-\alpha L) \leq 1$ is the loss of the ring, α is the intensity attenuation coefficient, ξ is the excess loss and L is the length of the ring. The angular frequency Ω in Eq. (1) is normalized to the Free Spectral Range (FSR) given by $FSR = c/n_{ef}L$, where c is the light speed in the vacuum. The intensity transmission coefficient defined as $T_{31} = |t_{31}(\Omega)|^2$ and the group delay defined as $\tau_{31}(\Omega) = -d\{\arg t_{31}(\Omega)\}/d\Omega$, are given by:

$$T_{31} = \frac{\xi^4 a + \xi^2(1-k) - 2\xi^3\sqrt{a}\sqrt{1-k}\cos(\phi+\Omega)}{1+\xi^2(1-k)a - 2\xi\sqrt{1-k}\sqrt{a}\cos(\phi+\Omega)}, \quad (2)$$

$$\tau_{31}(\Omega) = \frac{\xi^4 a - \xi^3\sqrt{a}\cdot\sqrt{1-k}\cos(\phi+\Omega)}{\xi^2(1-k) - 2\xi^3\sqrt{1-k}\sqrt{a}\cos(\phi+\Omega) + \xi^4 a} + \frac{\xi\sqrt{1-k}\sqrt{a}\cos(\phi+\Omega) - \xi^2(1-k)a}{1-2\xi\sqrt{1-k}\sqrt{a}\cos(\phi+\Omega) + \xi^2(1-k)a}. \quad (3)$$

By the addition of a second straight waveguide coupled to the ring, a four port device can be obtained as is shown in Fig. 1(b). Ports 1 and 4 are the inputs of the device while ports 2 and 3

are the outputs. In this way, it can be defined four transfer functions: $t_{31}(\Omega)$ and $t_{71}(\Omega)$ for the input at port 1, and $t_{35}(\Omega)$ and $t_{75}(\Omega)$ for the input at port 4. Due to the symmetry of the device the transfer functions $t_{31}(\Omega)$ and $t_{75}(\Omega)$ are similar, and the same happen with transfer functions $t_{71}(\Omega)$ and $t_{35}(\Omega)$. Moreover, $t_{31}(\Omega)$ has an analogous response that its counterpart in the two port ORR, so we only analyze the transfer function $t_{71}(\Omega)$, which is given by:

$$t_{71}(\Omega) = \frac{\xi_1 \xi_2 \sqrt[4]{a}\sqrt{k_1}\sqrt{k_2}\exp[j(\pi-\Omega/2-\phi)]}{1-\xi_1\xi_2\sqrt{1-k_1}\sqrt{1-k_2}\sqrt{a}\exp(-j\Omega)\exp(-j\phi)}. \quad (4)$$

From this equation, the intensity transmission coefficient, $T_{71}(\Omega)$, and group delay, $\tau_{71}(\Omega)$, can be obtained in a similar manner as presented for the two port device.

Since the main objective is to know the feasibility to build integrated tunable delay lines, it is necessary to analyze the response of a real device and comprehend the influence of the involved parameters. In that sense, numerical simulations were performed from Eqs. (1) and (4) considering that the system is composed by integrated waveguides of silicon dioxide and silicon nitride (SiO_2/Si_3N_4) with $n_{ef} = 1.48$ and $\alpha = 10$ dB/m. The default coupling factor was set as $k = 0.5$, the coupler insertion loss 0.1 dB (i.e. $\xi \cong 0.9886$) and the nominal radius of the ring was 6 mm. From these values, $\lambda = 1550.02$ nm for $N = 35996$, is one of the possible resonance wavelengths.

Figures 2(a) and (b) show the intensity transmission coefficient and group delay (normalized by the round-trip time $T_{RT} = n_{ef}L/c = FSR^{-1}$), for the two ports ORR in (a), and for the four ports ORR in (b). It can be seen from the magnitude response (upper side of the figure) that at the resonance frequency the two port device acts like a notch filter, while the four port device does like a band pass filter. However, both devices produce a delay group which is maximum around the resonance frequency, as is shown in the lower side of the figure.

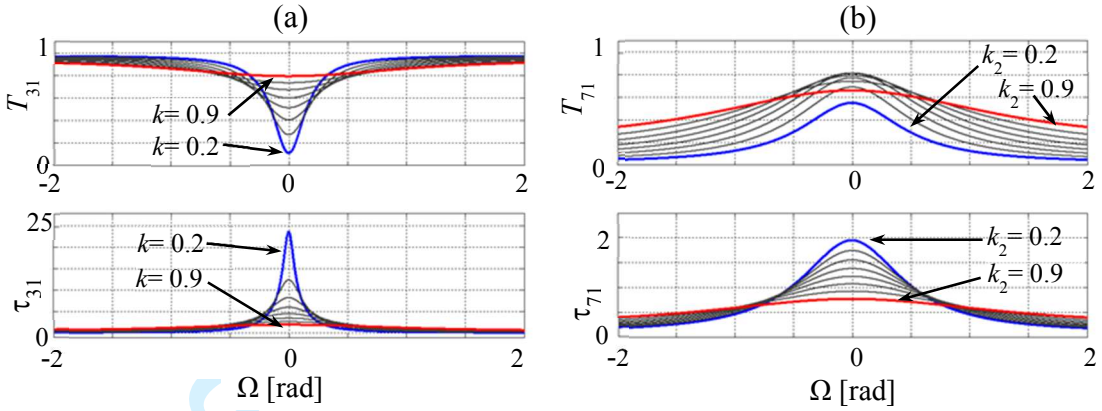

Fig. 2 (a) Response of the two ports ORR for k varying between 0.2 and 0.9, and (b) response of the four ports ORR for k_2 varying between 0.2 and 0.9 and k_1 = 0.5. Both figures show in the upper side the intensity transmission coefficient and in the lower side the normalized group delay for $\phi = 0$.

The influence of coupling factor over the response in both devices can be seen in Figs. 2(a) and (b) for the intensity transmission coefficient and group delay, where the parameter k and k_2 takes values from 0.2 to 0.9, being $k_1 = 0.5$ in the four port ORR. It can be seen from (a) (two port device) that the resonator is operating in the over-coupled region and by reducing the coupling factor, the intensity transmission coefficient and the group delay become more selective and sharp, i.e. the FWHM is reduced. By considering the four port device from figure (b), the intensity transmission coefficient has not a uniform evolution in the response for the analyzed variation of the coupling factor, due to two coupling factors are included in the response. Otherwise, the group delay shows a similar response that the two port ORR where the group delay is increased as k_2 is reduced. However, a significant difference for the simulated values is that the two port device has a response narrower than the four port device, and also the maximum reachable delay in the two port device is about 10 times higher than in the four port device. Moreover by increasing the peak value of the group delay also increases its selectivity and the

FWHM is reduced. Hence a committed relationship between the maximum delay to be implemented and its bandwidth is obtained, when only one ORR is employed.

Another control parameter is the phase shift ϕ introduced by a phase modulator included within the ring to change the resonance frequency. This can be inferred from Eqs. (1) and (4), which show that the influence of PM is analogous to a frequency offset. Due to the phase modulation has a similar effect for two- and four-port device, only the former is analyzed. The following simulations show the response of the device for values of the phase shift which ranges from 0 to 0.8π rad. These correspond to typical values obtained with thermo-optical phase shifters [20]. Figure 3(a) shows that the phase shift introduced into the ring has the effect of modifying the resonance frequency of the device, which can be observed in both the intensity transmission coefficient (upper figure) and the normalized group delay (lower figure). Also, the response demonstrates that the shape of the magnitude of the intensity transmission and the group delay is independent of the phase modulation and it only produces a frequency shift. This behavior can be useful for delaying signals that modulate several carriers at different wavelengths or, for instance, to make a fine tuning to correct small deviations that may appear during the implementation. Another important application arising from the response of the device is to implement group delays with high bandwidth, by using several rings tuned to different resonance frequencies. It should be noted that, as any real device, the PM introduces an insertion loss which has been considered in the numerical simulation through the loss parameter of the waveguide

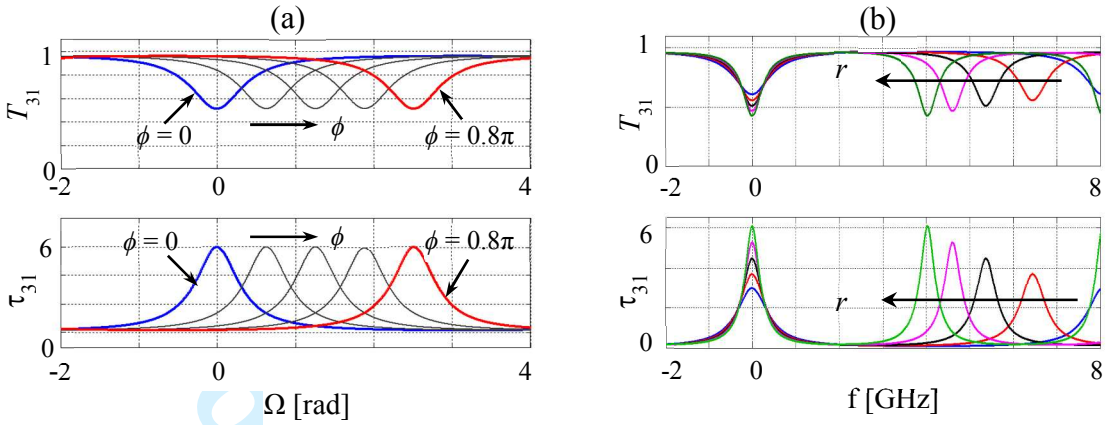

Fig. 3 Intensity transmission coefficient (upper side) and normalized group delay (lower side) for (a) variable phase modulation for ϕ = 0, 0.2π, 0.4π, 0.6π and 0.8π, and (b) variable radii (or length of the ring) for 4, 5, 6, 7, and 8 mm. The variation of ϕ produces a frequency shift in the response and L modifies the FSR and the shape (peak value and FWHM) of the response. The coupling is k = 0.5.

Finally, to analyze the effects of varying the length of the ring, different radii were considered ($L = 2\pi r$, where r is the radius). Figure 3(b) shows the results when the radius takes the following values: 4, 5, 6, 7, and 8 mm, where the group delay was normalized to the greater T_{RT} of the interval, to appreciate the relative differences between the peak values and widths. Unlike the previous cases, it can be seen that the length of the ring has a significant impact on the FSR of the response and that smaller radii correspond to higher FSRs. Therefore, for broadband applications it is desirable to make the device as small as possible which justify the use of devices based on integrated optics instead of fiber-optic ring resonators. Furthermore, as it is expected, higher bandwidths correspond to lower peak delays because smaller dimensions mean shorter round trip times.

To summarize the obtained results, we introduce Table 1 where the control and constructive parameters are compared, by taking into account the capability to adjust the time delays, the free-

spectral range, the intensity transmission coefficient in the pass/stop -band, and the difficulty to implement this facility.

Table 1 Comparison of how parameters affect the ORR.

	n_{ef}	EL	L	k	ϕ
τ peak value	Low	Low	High	High	No
FSR tunability	Low	No	High	No	No
Resonance frequency	Low	No	Medium	No	High
T variation	Low	Low	Medium	High	No
Implementation difficulty	High	Low	High	Medium	Medium

The coupling factor, k, the phase modulation, ϕ, and the length of the ring, L, are the better control parameters to govern the response of the device. However, at difference of k and ϕ, the variation of L is difficult to implement in a real device. By means of the coupling factor is possible to adjust the magnitude of the delay group, while through the phase modulation can be adjusted the resonance frequency. Both parameters can be easily controlled by the thermo-optical effect. This consists in changing the refractive index of the waveguide by means of a temperature change. Thus, optical phase shifters can be implemented by small metal electrodes or thin-film heaters, which modify the refraction index of the waveguide when a current is circulating through them. This thermo-optical phase shifter has been used to tune the temperature of various waveguide devices [20,21]. The variable coupling k is reachable with a Mach-Zehnder interferometer which is implemented with two 3 dB couplers and an optical phase shifter in one of its branches. This technique is simple, introduces few additional losses in the waveguide and provides tuning speeds faster than microseconds, acceptable value for most beamforming applications.

2.1 Topologies

In previous sections it was shown that the bandwidth of the group delay generated by two port and four port ORRs is inversely proportional to its peak value, which means that wideband signals cannot be delayed in large quantities without significant distortion. This means that, if the group delay is not constant over the entire bandwidth of the signal, some of the frequency components will be delayed more than others. Considering an example of a delay line applied to a beamforming system, different delays also involve distortion of the radiation pattern, and therefore the uniformity of the response is an issue that must be taken into account. In order to increase the bandwidth of the generated delay lines we propose to implement structures with more than one ORR: cascaded ORRs and stacked ORRs (or ring lattice structure).

2.1.1 Cascade of ORRs

To achieve a flat group delay characteristic within a wider bandwidth we analyze the results of cascading several ORRs. In this topology, the rings are connected one next to the other, where each ring does not interact with neighbor rings, i.e. there is no coupling between them and the light only propagates through the input/output ports. This topology can be seen in Fig. 4(a) where a cascade of three identical rings with control parameters k and ϕ, is shown.

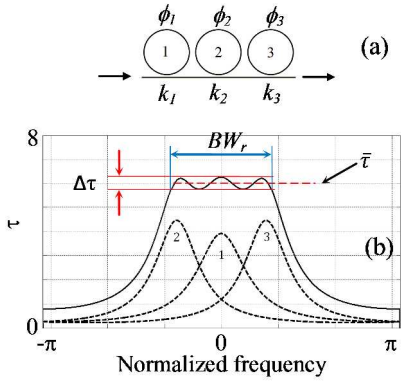

Fig. 4 Cascade of three ORRs: (a) Schematic (b) Individual and resultant delays.

In this configuration, as the input of each stage is the output of the previous one, the resulting transfer function is obtained as the product of the individual transfer functions (given in Eq. (1)), and the total normalized group delay as the sum of the individual delays. In particular, if N is the number of cascaded rings and they have identical construction parameters, the Eqs. (5) and (6) describe the transfer function and normalized group delay of the system:

$$t(\Omega) = \prod_{i=1}^{N} \left[\frac{\xi\sqrt{1-k_i} - \xi^2\sqrt{a}\exp(-j\phi_i)\exp(-j\Omega)}{(1-\xi\sqrt{1-k_i}\sqrt{a}\exp(-j\phi_i)\exp(-j\Omega))} \right], \tag{5}$$

$$\tau(\Omega) = \sum_{i=1}^{N} \left[\frac{\xi^4\, a - \xi^3\sqrt{a}\sqrt{1-k_i}\,\cos(\phi_i+\Omega)}{\xi^2\,(1-k_i) - 2\,\xi^3\sqrt{1-k_i}\sqrt{a}\,\cos(\phi_i+\Omega) + \xi^4\, a} + \frac{\xi\sqrt{1-k_i}\,\sqrt{a}\,\cos(\phi_i+\Omega) - \xi^2\,(1-k_i)\,a}{1 - 2\,\xi\sqrt{1-k_i}\,\sqrt{a}\,\cos(\phi_i+\Omega) + \xi^2\,(1-k_i)\,a} \right]. \tag{6}$$

Figure 4(b) shows the individual and the total normalized group delays. It can be seen that the peaks of the individual delays give rise to small variations with a peak-to-peak value defined as the ripple of the group delay $\Delta\tau$. In the same figure we define the bandwidth of the ripple, BW_r, as the frequency range where the value $\Delta\tau$ is satisfied, and the average value of the group delay, $\bar{\tau}$, in the defined bandwidth. While the small variations $\Delta\tau$ are inevitable and depend on the peak value and separation of the individual responses, they can be reduced to values that are considered acceptable within a certain bandwidth that depends on the number of ORRs used. This way, if the coupling factor k and phase shift ϕ for each ORR are properly chosen, an approximately flat response in a wide range of frequencies may be obtained.

The issue to be solved at this point is the adopted strategy to control the response of the system from the control parameters of each ring. An advantage of using this topology is that the individual responses of the elements composing the system are independent, simplifying, in this way, the control of the overall response. In Sec. 4 a control strategy for determining the values of the parameters that allows obtaining an approximately flat response in a cascade of ORRs is presented.

2.1.2 Ring Lattice

In contrast with the cascaded ORRs, in this configuration adjacent rings are coupled together, thus the system response cannot be obtained easily from the response of a single ring. The coupling between rings is implemented in the same manner as in the case of a four ports ORR, that is, by using an additional variable coupler within each loop. In this case, the guide at which the light is coupled is not straight but has a ring shape, which constitutes a second stage of the structure. This procedure can be extended to N stages, which form the ring lattice. Figure 5 shows a lattice consisting of three rings ($N = 3$) and the corresponding signals propagating in the forward ($F_0,..,F_N$) and reverse ($R_0,...,R_N$) directions. Also, the input electric fields, E_{i1} and E_{i2}, and the outputs, E_{o1} and E_{o2}, are shown.

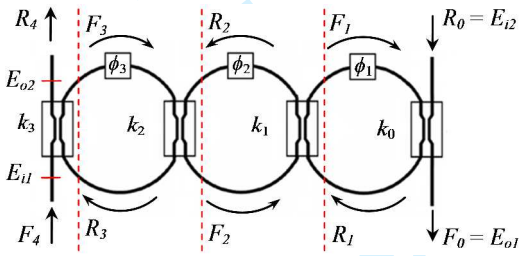

Fig. 5 Ring lattice composed of three ORRs.

In order to analyze the ring lattice response, we follow the mathematical fundaments presented in [22]. The matrix method allows obtaining the transfer function of a whole system which is formed by individual stages or subsystems. As can be seen in Fig. 5, the stages comprised in the system are separated by dotted lines, and each stage is composed of a coupler, a phase modulator and a portion of waveguide. In this way, if nth-stage is characterized by a specific transfer matrix, Φ_n with $n = 0$ to N, the complete transfer matrix is calculated as the product of the individual ones, i.e.

$$\begin{bmatrix} F_{n+1}(z) \\ R_{n+1}(z) \end{bmatrix} = \Phi_n \begin{bmatrix} F_n(z) \\ R_n(z) \end{bmatrix}, \tag{7}$$

$$\Phi_n = \frac{1}{-j\sqrt{k_n}} \frac{1}{\sqrt{\zeta_{n+1}}} \begin{bmatrix} 1 & -\sqrt{1-k_n} \\ -\sqrt{1-k_n}\zeta_{n+1} & -\zeta_{n+1} \end{bmatrix}, \tag{8}$$

where $z = \exp(j\Omega)$ and the parameter $\zeta_n = \sqrt{a}\exp(-j\phi_n)z^{-1}$ defines the properties of the ring such as attenuation, phase modulation and time delay in the waveguide. The input-output relation for a ring lattice of N stages can be established by means of the total transmission matrix as $\Phi_{TOT} = \Phi_N \Phi_{N-1} \ldots \Phi_0$ and the transfer functions $t_{11} = E_{o1}/E_{i1}$ and $t_{21} = E_{o2}/E_{i1}$ that relate the input and output electric fields are obtained as:

$$t_{11}(z) = \frac{F_0(z)}{\sqrt{\zeta_{N+1}} F_{N+1}(z)} = \frac{(-j)^{N+1}\sqrt{\sigma_N \exp(-j\phi_{tot})}\, a^{N/2} z^{-N}}{A_N(z)}, \tag{9}$$

$$t_{21}(z) = \frac{R_{N+1}(z)}{\zeta_{N+1}\, F_{N+1}(z)} = \frac{B_N(z)}{A_N(z)}, \tag{10}$$

depending on which output, one or two respectively, is considered. $\phi_{tot} = \phi_1 + \cdots + \phi_N$, $A_N(z)$ and $B_N(z)$ are polynomials in variable z^{-1} which are obtained from the elements (1,1) and (2,1) of the total transfer matrix Φ_{TOT} mentioned before.

It is intuitive to think that in the lattice configuration the selectivity of the response increases, because the resonating light must satisfy more conditions than for a single ring. In this way, each ring incorporated to the lattice structure modifies the resonance condition of the previous one, because it introduces a phase which depends of the frequency of the signal. This is the cause for which more peaks appear as resonances when the number of coupled rings is increased, as will be shown in the next figures.

Because of the large number of variables and degrees of freedom of the system, it was decided to perform general simulations for some specific situations that are illustrative. It allows to analyze the performance and to characterize the transmission and group delay of the ring lattice. In addition, it was found through simulations that the effect of the phase modulation ϕ is

complex to predict and does not provide improvements on the shape of the response, such as broadband and flat delays. Therefore, all phase modulations have been considered equal to zero in the following analysis. For the numerical simulations two cases have been developed: the first one, when $k_0 = 0$ and there is no coupling to the second straight guide at the end of the lattice, $t_{21}(\Omega)$ is analyzed. In this case, the device behaves as a two-port network. The second one, when $k_0 \neq 0$, the two transfer function are not nulls and the device behaves as a four-port network. In this case only $t_{11}(\Omega)$ is investigated because $t_{21}(\Omega)$ produces similar results as obtained in the first situation. The simulations were realized employing devices with the same characteristics as those regarded in the previous cascade structure. At the same time, three different operating conditions were analyzed: (*i*) all couplings have the same value; (*ii*) the coupling increases with each added ring; and (*iii*) the coupling decreases with each added ring. In all cases, the graphics show the variation of the response to a simultaneous increment/reduction of all coupling factors in 0.1.

A. Two port device ($k_0 = 0$):

Figures 6(a) and (b) show the intensity transmission coefficient and the group delay corresponding to the transfer function $t_{21}(\Omega)$ for the case in which all the coupling factors are equal, i.e. $k_3 = k_2 = k_1$. Red lines correspond to the case $[k_3\ k_2\ k_1] = [0.1\ 0.1\ 0.1]$, while blue lines stand for the case [0.7 0.7 0.7]. Additionally, Figs. 6(c) and (d) show the same curves for the case where the coupling factor of each new added ring is lower than the previous one, i.e. $k_3 > k_2 > k_1$ by an account of 0.1. In this instance, red lines correspond to the coupling factors $[k_3\ k_2\ k_1] = [0.3\ 0.2\ 0.1]$, while blue lines stand for the case [0.9 0.8 0.7]. The figures considering the situation in which the coupling factor of each added ring is greater than the previous one were omitted because the system response is very similar to the obtained in the first case, where all coupling factors are equals.

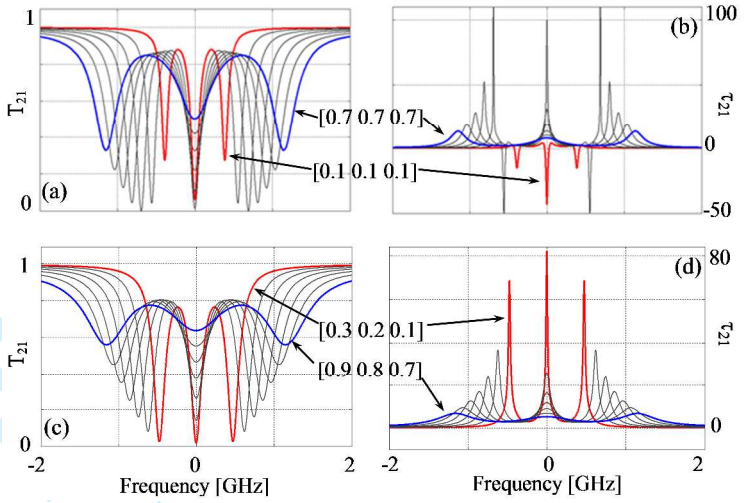

Fig. 6 Intensity transmission coefficient and group delay for similar coupling factors, (a) and (b), and increasing coupling factors, (c) and (d).

From the figures it is possible to see that the number of peaks of resonance is increased with respect to the response of a single ring, and matches the number of coupled rings. In the two presented cases, the intensity transmission coefficient exhibits valleys, which become less selective and they separate from each other as the coupling factors are increased. However, the relative amplitudes of these valleys are few different in both cases. On the other hand, the group delay exhibits very sharp and selective peaks which reduce its amplitudes and separate its resonance frequencies as the coupling factors increase. The relatively large variations of the response within the device bandwidth are an inconvenient if it is desired to implement delays lines for broadband signals. However, because the signal propagating in the ring lattice structure of two ports has to travel from the input port, at the left side, to the right side and then go back to the output port, at the left side again, the time delay can be longer than in a cascade structure. From Figs. 6(b) and (d) can be observed that the obtained delays take values about one hundred round-trip times, while for the cascade ring the delay takes values about ten round-trip times, for the considered structures based on three ORRs.

B. Four port device ($k_0 \neq 0$)

As it was mentioned before, in this case we analyze the transfer function $t_{11}(\Omega)$ to the second straight waveguide, thus the output is a fraction of the resonating light within the rings. Figures 7(a) and (b) show the intensity transmission coefficient and the group delay for the case in which all the coupling factors are equals. Red lines correspond to the case $[k_3\ k_2\ k_1\ k_0] = [0.1\ 0.1\ 0.1\ 0.1]$ with increments of 0.1 up to reach the blue lines corresponding to the case [0.6 0.6 0.6 0.6]. It is noted that the intensity transmission coefficient and the bandwidth increase when the coupling factors become greater. Moreover, the delays obtained are less selective and with lower peak values than in the two-port configuration.

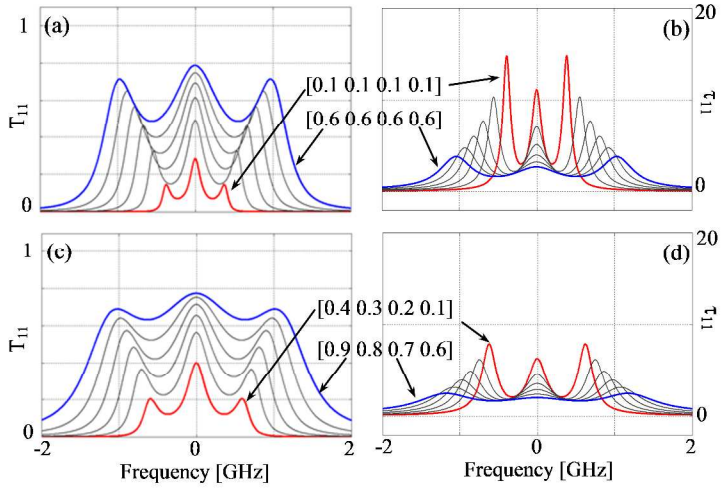

Fig. 7 Intensity transmission coefficient and group delay for similar coupling factors, (a) and (b), and increasing coupling factors, (c) and (d).

The case in which the coupling factors range from [0.4 0.3 0.2 0.1] to [0.9 0.8 0.7 0.6] is shown in Figs. 7(c) and (d), and the results are identical to the obtained when coupling factors decrease with each added ring, therefore the figure of the latter case was omitted. From the figures can be observed that the intensity transmission coefficient has a similar behavior although it has less selective peaks than in previous case. On the other hand, the variations or

ripple within the bandwidth of both the intensity transmission coefficient and group delay, are smaller than in the case where all the coupling factors are equals. However, these variations are still not negligible and it should be required to control at least the coupling factor of every ring in order to obtain broadband delay lines with flat response. This control strategy, according to the previous analysis, results more complex to implement than the corresponding to the structure given by the cascade ORRs.

In summary, the ring lattice configuration proved to be capable of generating large delays but with the disadvantage that the response given by the intensity transmission and the group delay are not flat and present great deviations in the bandwidth of interest. Reducing these variations requires a complex control strategy because the behavior of the response to changes in the adjustable parameters is not direct. It depends on complicated mathematical functions as were presented. In that sense, the cascading of ORRs topology is more effective and simple to control in order to obtain uniform delays and large bandwidths as required in broadband optical beamforming applications. However, the lattice structure may be useful for other applications such as those requiring the implementation of large delays and frequency selectivity (small bandwidths). For example, delays of about 400 T_{RT} with FWHM of 5 MHz can be obtained.

3 Delay Lines Control Strategy

Based on the previous analysis, we choose to use the cascade ORRs system because it is easier to implement a control strategy and allows obtaining uniform delays in a broad working bandwidth. In this section we will deal with the problem which consists of determining and estimating the values of the control parameters required to achieve the desired group delay characteristics, i.e. mean value, ripple and bandwidth. The proposed strategy has to be as simple as possible because the delay lines are designed to work in a real beamforming network. The idea consists in

obtaining through numerical simulations a set of functions that relate the control parameters of the system, under approximately flat response, with the average delay in the band of frequencies of interest. Thus, it is possible to implement a lookup table in which the values of the control parameters of the ORRs are obtained from the required time delays, being this solution simple to implement in high-speed electronic devices. Additionally, the results allow estimating some characteristics of the system response, such as bandwidth, attenuation, among other.

In the simulations were considered ORRs of 12 mm diameter, with effective refractive index $n_{ef} = 1.48$, and loss $\alpha = 10$ dB/m. These values correspond to those typically obtained in SiO_2/Si_3N_4 waveguides. From these values, it is possible to determine the $FSR = 5.38$ GHz and the $T_{RT} = 185.98$ ps. Figure 8 shows the flux diagram of the procedure to carry out the control strategy, which is explained in the following paragraphs.

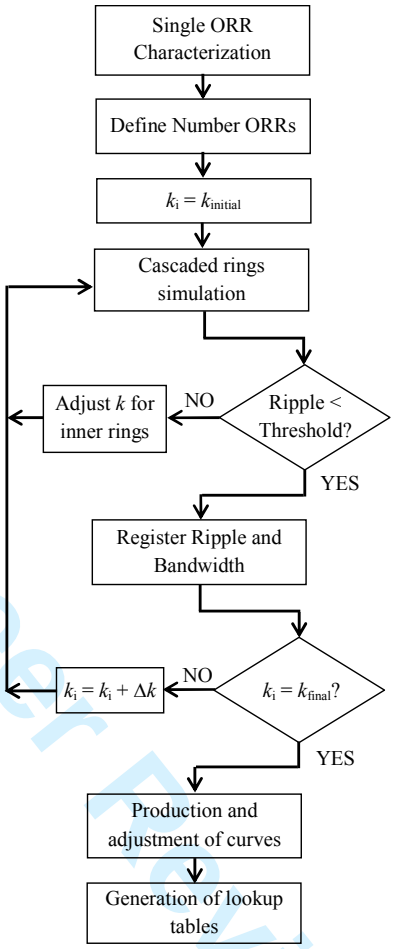

Fig. 8 Control strategy represented in a flux diagram.

First, the group delay as a function of the normalized frequency for one ORR is calculated. From this expression we can calculate the peak delay and the FWHM of the response for different values of coupling coefficient. These characteristics are shown graphically in Figs. 9(a) and (b), where the coupling factor ranges from $k_{initial} = 0.2$ to $k_{final} = 0.9$ in steps of $\Delta k = 0.05$. Lower values for k were not considered to avoid the sub-coupled area due to the undesired behavior of the group delay. From these figures, it can be verified the tradeoff established between the peak value and the bandwidth of the group delay, i.e. larger values of peak delay correspond to smaller widths of the response, and vice versa. From Fig. 9, given a value of

coupling factor we can know the contribution to the group delay for the corresponding ring. Furthermore, the FWHM will be used to determine the spectral separation between adjacent ORRs in order to dynamically adjust some characteristics of the response, such as the total bandwidth and ripple of the delay.

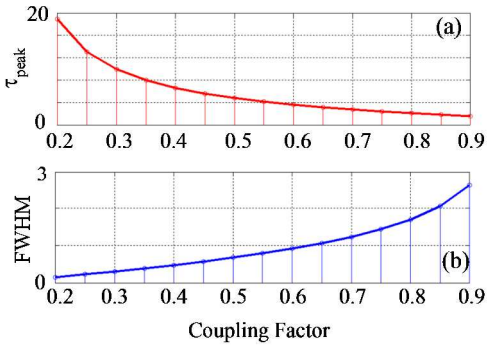

Fig. 9 Single ORR Characterization: (a) Peak value vs *k*, and (b) FWHM vs *k*.

The next step consists in defining the number of rings to cascade, and this is determined by taking into account several issues. On the one hand, the bandwidth in which we wish to operate can be increased by cascading individual rings whose response is slightly shifted in frequency by controlling the phase modulation coefficient (as seen in the Fig. 3(a)); on the other hand, if the number of rings increases it also increases the manufacturing complexity and hence the cost of the device and the necessary control circuit. In the following analysis we have arbitrarily chosen the odd number 5, but such decision will depend on each application.

Initially we set the phase modulation coefficient of each ring in a way such that adjacent rings are separated in frequency by half FWHM, as is shown in Fig. 10(a). This choice reduces the degrees of freedom in addition to minimizing the ripple of the resulting group delay. Besides, the coupling coefficients of all rings are initially fixed with the same value. It can be seen in Fig. 10(b) where the resulting group delay and the contribution of each ring, are shown.

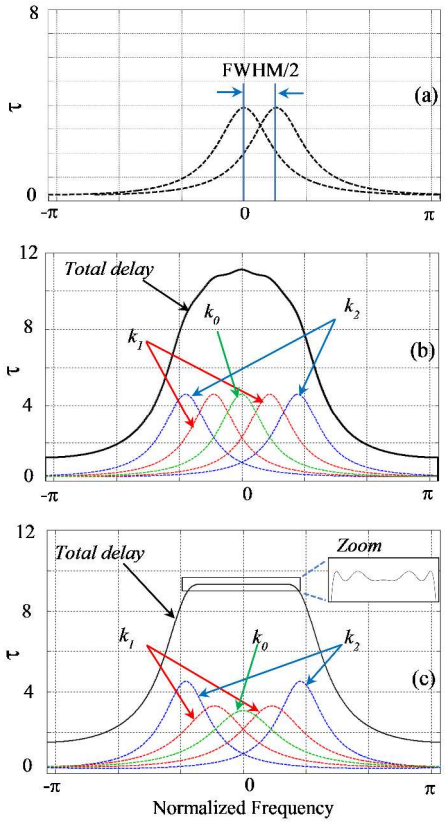

Fig. 10 (a) Spectral separation between adjacent ORRs responses. (b) Resulting delay at the initial state. (c) Resulting delay at final state.

Then an iterative numerical simulation begins, which is repeated for each value of the coupling factor *k* within the considered range 0.2 - 0.9. As can be seen in Fig. 10(b) where the initial state of one simulation is shown, all rings provide a considerable delay at the resonance frequency, resulting in a bell-shaped response. It is evident, therefore, the need to act on the responses of each ring in order to obtain an approximately flat group delay with the desired average value. Consequently, it is proposed to reduce the peak delays closer to the center and keep unchanged the two outermost. As is evident from the Fig. 9(a), a reduction of the peak delay may be obtained by increasing the coupling factor of the corresponding ORR. Therefore, k_0

and k_1 (inner rings factors) were incremented to reduce the peaks of the corresponding delays, while k_2 (factor of the outer rings) was maintained at the same value.

The procedure can be summarized as follows: increasing the coupling factor of the central ring until a desired delay value is achieved, then continue with the adjacent rings, and so on for each pair of rings until reaching the extremes of the structure. In the case of five rings, first k_0 is increased and then k_1, observing the ripple status after each modification. This iterative process finishes when a response with bounded and uniform ripple within the bandwidth of interest is obtained. Figure 10(c) shows the approximately flat response obtained in the final state of the numerical simulation. The zoom in the area of interest allows to observe the resulting small ripple of the group delay.

Once the condition of required small ripple is reached, the average intensity transmission coefficient, average delay, ripple and ripple bandwidth are obtained and saved. Finally, the value of the initial coupling factor is incremented and the procedure described above is repeated until reaching the last value in the selected range. The obtained results for the case of five cascaded rings will be discussed in the next section.

4 Results

4.1 Intensity Transmission Coefficient and Working Range

Figure 11(a) shows the intensity transmission coefficient as a function of the average delay in the band of interest. The system behaves like a filter whose intensity transmission decreases as the implemented delay is increased. This feature has to be considered carefully because it can be used to determine the range of delays for which the output signal has a power level high enough that allows detection in the receiver side. In that sense, we selected a minimum intensity

transmission of 20 % in order to get a suitable signal to noise ratio. Therefore, the maximum delay $\bar{\tau}_{max}$ is determined by intercepting the intensity transmission curve with a horizontal line corresponding to 0.2; and the minimum delay $\bar{\tau}_{min}$ is determined by practical limitations of the implementation, since small delays correspond to coupling factors close to unity, which are difficult to achieve. Hence, the working range of the system is shown as a shaded region in Fig. 11, as well as the boundaries $\bar{\tau}_{min}$ and $\bar{\tau}_{max}$. For the simulated system values, where T_{RT} = 185.98 ps, the working range covers delays from 929.9 ps to 2417.74 ps.

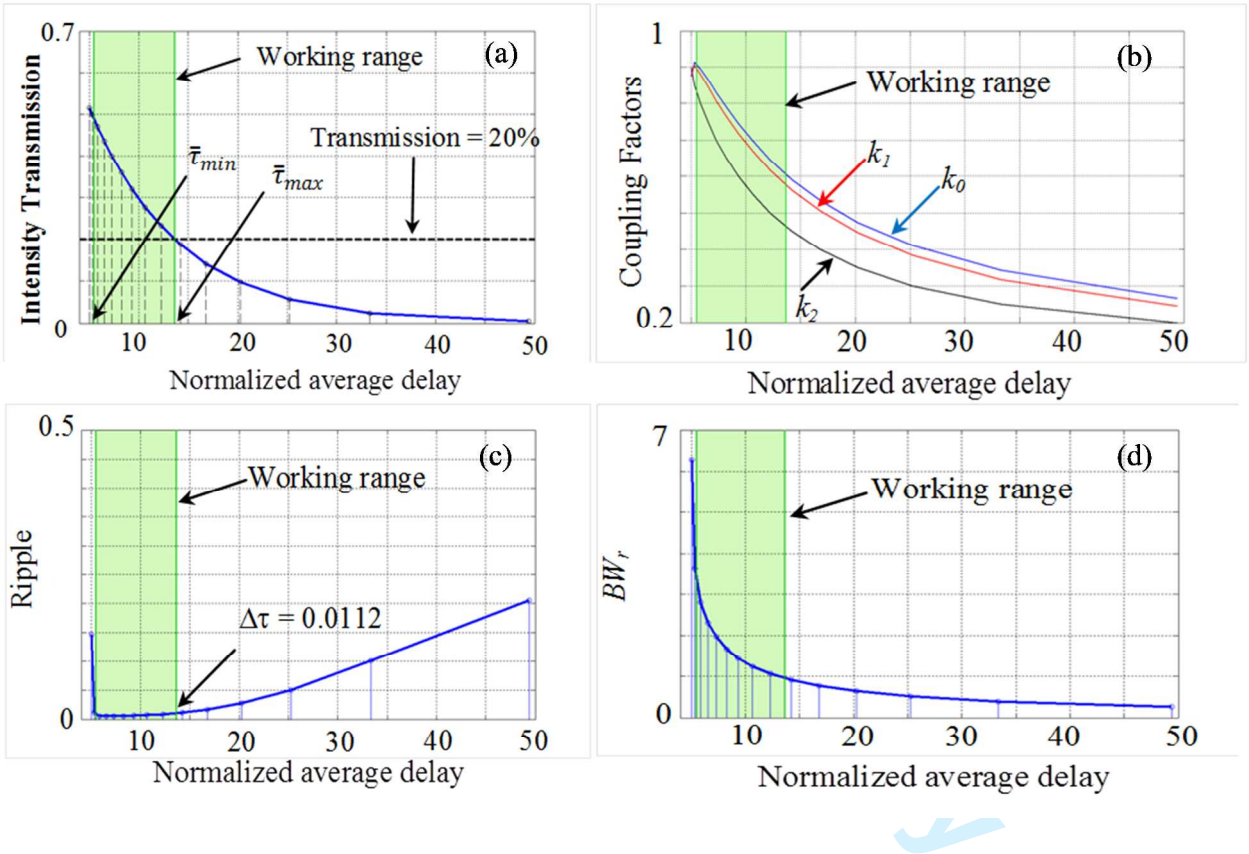

Fig. 11 (a) Average intensity transmission coefficient vs. average delay. (b) Coupling factors vs. average delay. (c) Ripple vs. average delay. (d) Ripple bandwidth vs. average delay.

4.2 Coupling Factors

Figure 11(b) shows the variation of the three coupling factors involved in controlling the five rings of the system as a function of the average delay. Notice that all have a similar decreasing

variation in an approximately exponential way when $\bar{\tau}$ increases. Since these curves were obtained under an approximately flat delay response, by fitting them with a suitable numerical method the values of the coupling factors required to implement any flat delay in the considered range can be obtained. In particular, for the proposed system, coupling factors take values between 0.464 and 0.907 within the operating range.

4.3 Ripple

As mentioned above, the data obtained from simulations allow to further characterize the response of the system. Figure 11(c) shows the ripple $\Delta\tau$ as a function of the normalized average delay. It can be seen that for relatively small delays within the working range, the ripple in the band of interest grows very slowly and can be considered constant.

The fact that the ripple is small and uniform within the bandwidth of work is desirable because this way all frequency components of a given input signal may be affected by approximately the same delay, minimizing the distortion. For longer delays, however, an increase of the ripple is evident and certainly not negligible. In the particular case of the proposed system, the denormalized ripple reaches a maximum value of 2.08 ps, representing approximately 0.09% of the corresponding average delay to that condition.

4.4 Ripple Bandwidth

Ripple bandwidth, BW_r, defined as the frequency range in which the variations are less than or equal to $\Delta\tau$, is another of the characteristics that was obtained in each numerical simulation, and from an interpolated curve it is possible to obtain it for any value of average delay within the considered range. The curve obtained for BW_r as a function of the normalized average delay is presented in Fig. 11(d) and shows a decreasing variation with increasing $\bar{\tau}$. This means that for a

given application, the minimum bandwidth that the device can provide is determined by the maximum delay to be obtained. When the frequency axis is denormalized with respect to the free spectral range, we find that the ripple bandwidth varies between 0.82 GHz and 2.85 GHz within the working range, and the corresponding values for $\Delta\tau$ are 2.08 ps and 1.79 ps. Notice that the bandwidth can be easily increased by incorporating ORR in cascade an following the same procedure to control the characteristics of the delay group.

4.5 Practical Application and Validation

The fitting curves obtained through simulations, which are shown in the preceding figures, can be used to generate a couple of lookup tables that allow implementing in real time, the desired time delays. The first table is generated from the curves of Fig. 11(b) and allows to obtain the coupling factors for a given average delay value. The second table is obtained from the curve of Fig. 9(b) and determines the value of the phase modulation needed to tune the center frequency of the rings, for the same average delay.

For example, if one is interested in generating an average delay of 1.86 ns (i.e. 10 T_{RT}) with deviations lower than 2 ps on microwave signals with bandwidth between 0.8 and 2.8 GHz, the proposed system of five cascaded ORRs would be adequate. In this case, the first table yields the values $k_0 = 0.72$, $k_1 = 0.69$ and $k_2 = 0.57$. Then, the value of k_2 is used as input to the second table and defines a spectral separation between adjacent rings of 0.36 GHz, which corresponds to a phase modulation of $\phi_1 = 0.42$ rad for the inner rings and $\phi_2 = 0.84$ rad for the outer ones. Thus, all control parameters required to implement the desired average delay are determined. Moreover, the curves presented in Figs. 11(c) and (d) provide the characteristics of ripple and ripple bandwidth of the response. For the proposed example, the values obtained are 1.26 ps and 1.15 GHz, respectively. As can be seen, the proposed strategy is extremely simple and easy to

implement in a DSP or FPGA device, allowing the generation and characterization of controlled delays for large bandwidth applications.

In order to validate both, the obtained results and the need of controlling the ripple value of the generated delays, we show the irradiation pattern of a 4-element linear array of isotropic sources for a steering angle of -45 degrees. Figure 12 shows the required delays, obtained by applying the strategy presented above in each branch of the system, as a function of the frequency. To evaluate the influence of the delays ripple on the radiation pattern, different frequencies within the ripple bandwidth were selected, and a pattern with the corresponding delay values was generated in each case. In particular, twenty equally spaced frequencies, indicated with red vertical lines in the figure, were chosen. An inset figure shows how the delay for each selected frequency varies in the case of the branch one. Due to the symmetry of the implemented delays with respect to the microwave frequency carrier (indicated as 0 GHz on the horizontal axis) it is enough to analyze the radiation patterns corresponding to positive frequencies because those obtained for the negative frequencies produce identical results.

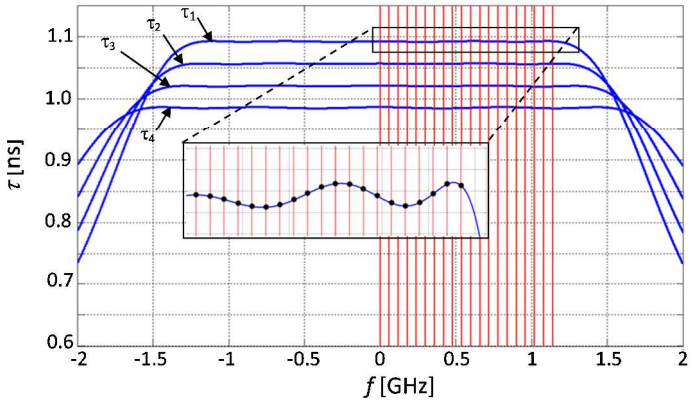

Fig. 12 Delays implemented for each branch of the OBF system.

Thus, for each of the indicated frequencies four delay values are determined, one for each branch of the system, which should ideally steer the radiation pattern with the desired angle (–45º). However, due to the variations of delays, the steering angle exhibit deviations. Figure 13(a) shows in solid red line the radiation pattern obtained for each selected frequency and in dashed blue line the ideal pattern for a 10 GHz carrier microwave signal. The main lobe, which is better appreciated from the inset figure, exhibits very small variations of the steering angle. The power radiated by the secondary lobe of the pattern shows variations produced by the interference pattern of N point sources that depend on the ratio between the wavelength of the signal (or equivalently the frequency) and the distance between the antennas. This variation of the radiation pattern is independent of the method used to control the delays of the signals due to the non-negligible bandwidth of the signal. In order to quantify the variations of the main lobe, the angle at which the radiated power is maximum for each simulated radiation pattern was determined. Therefore, the mean value and the standard deviation were calculated from the simulations, which are given by –45.0º and 0.5º, respectively.

With the aim to make a comparison, the same analysis is performed using ideal optical phase shifters (PS) instead of true time delays. Figure 13(b) shows the obtained radiation patterns considering the same bandwidth than in previous case. As can be seen, the variation of the radiation angle of the main lobe is higher than in the previous case based on TTDs. In the phase shifter based system the average angle is shifted to –45.2º and the standard deviation is 2.0º, which is four times higher.

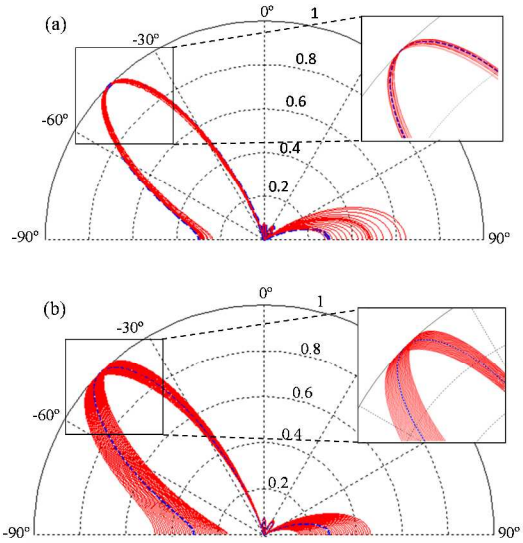

Fig. 13 Radiation patterns obtained for different frequencies within the ripple bandwidth for an OBF system based on (a) TTD implemented with ORRs, and (b) ideal phase shifters.

5 Conclusion

In this article we presented an analysis for implementing photonic devices suitable for the generation of delay lines of RF and microwave signals. The final objective is to generate true time delay lines (TTD) to be applied in an optical beamforming (OBF) system. In a previous work we presented FBG-based TTD and how their impairments affect the response of OBF system [23]. However, the need for integrating the devices to reduce the size and weight, and simplify the control system, made the research and develops line to turn to the integrated ORR.

In the first part, it was demonstrated how the coupling factor and the phase modulation within the ORR are suitable to control the delays. These parameters allow the modification of the peak value and the resonance frequency of the response. However, the resulting bandwidth is inversely proportional to the delay peak value, generating a tradeoff relationship.

To achieve a flat response in a wider bandwidth (a few GHz for 5 ORRs), different configurations and topologies that use multiple devices were proposed. The most appropriate in

complexity and ability to reduce the ripple proved to be the cascading of ORRs, by controlling the coupling factor and the phase modulation for each ring. A strategy to control the delay was proposed and the procedure was described in detail. In addition to determine the system control parameters required to implement a given average delay, the results obtained also served to characterize the response. To validate the proposal an example was presented considering a system comprised of a cascaded of 5 ORRs implemented using SiO_2/Si_3N_4 waveguides. The obtained bandwidth varies between 0.82 GHz and 2.85 GHz and the ripple is kept less than 2.08 ps. The strategy presented has the advantage of being very simple to implement with DSP facilities and does not require complex calculations. This feature makes the proposed method ideal for real time applications in optical beamforming systems. The results are validated by comparing the radiation pattern of a 4-element linear array of isotropic sources for two different systems: the former uses ORRs and the control strategy presented in this paper, and the second one uses phase shifters to control the phase of the signals feeding the antennas. Results show that for a steering angle of –45º, the system based on TTD-ORRs produces a deviation about four times lower than phase shifter based system.

Finally, the proposed method is applicable to an arbitrary number of rings as can be seen from the flowchart shown in Figure 8. However, there are practical limitations resulting from the ability to manufacture N cascaded rings and corresponding thermal controls, for adjustment of both the coupling and phase modulation. Thus, there is a compromise between the required bandwidth and the number of rings that may be cascaded. Furthermore, the maximum system bandwidth and the number N of cascaded rings are limited by the Free Spectral Range of the ORRs.

Acknowledgements

Sebastian Rabal is fellowship of Scientific Research Commission of the Buenos Aires Province (CIC PBA). Since 2012 is with Centro de Investigaciones Ópticas (Universidad Nacional de La Plata - CONICET La Plata – CIC PBA), Camino Centenario y 506, La Plata, Bs. As. (1900), Argentina (e-mail: srabal@ciop.unlp.edu.ar).

Laureano A. Bulus Rossini is a researcher of the National Council of Scientific and Technical Research (CONICET) and Professor at Instituto Balseiro in Telecommunication Engineering. Since 2014 is with Instituto Balseiro (CNEA - Universidad Nacional de Cuyo) Av. Bustillo 9500, S. C. Bariloche (8400) RN, Argentina (e-mail: lbulus@ib.edu.ar).

Pablo A. Costanzo Caso is a researcher of the National Council of Scientific and Technical Research (CONICET) and Professor at Instituto Balseiro in Telecommunication Engineering. Since 2014 is with Instituto Balseiro (CNEA - Universidad Nacional de Cuyo) Av. Bustillo 9500, S. C. Bariloche (8400) RN, Argentina (e-mail: pcostanzo@ib.edu.ar).

References

[1]. J. E. Heebner, V. Wong, A. Schweinsberg, R. W. Boyd, and D. J. Jackson, "Optical Transmission Characteristics of Fiber Ring Resonators," *IEEE J. Quantum Electron*. **40**(6), (2004) pp.726-730.

[2]. S. Tedjini, "Theoretical & Experimental Study of Single Mode Fiber Optical Ring Resonators for Microwave Applications," *Microwave Symposium Digest, 1995, IEEE MTT-S International*, (1995) pp.1491-1494.

[3]. G. S. Pandian, F. E. Seraji, "Optical pulse response of a fiber ring resonator," *Proc. J IEE.* **138**(3), (1991) pp. 235-239.

[4]. Y. Shi, H. Yang, C.M. Okonkwo, A. M. J. Koonen and E. Tangdiongga, "Optical frequency multiplication using fibre ring resonator," *Eelctron. Lett*. **46**(11), (2010) pp. 781-783.

[5]. P. A. Costanzo Caso; S. Granieri; A. Siahmakoun, "Optical Leaky Integrator with Inverted and Non-inverted Accumulation," *Microw. Opt. Technol. Lett.* **53**(9), (2011) pp. 2034-2037.

[6]. E. Reeves; P. A. Costanzo Caso; A. Siahmakoun, "Theoretical Study And Demonstration Of Photonic Asynchronous First-Order Delta-Sigma Modulator For Converting Analog Input To Nrz Binary Output," *Microw. Opt. Technol. Lett*., **53**(3), (2015) pp. 574-578.

[7]. P. A. Costanzo Caso, Y. Jin, S. Granieri and A. Siahmakoun "Optical bistability in a Nonlinear SOA-based Fiber Ring Resonator," *J. Nonlinear Opt. Physics Materials*. **20**(3), 281-292 (2011).

[8]. C. G. H. Roeloffzen, L. Zhuang, R. G. Heideman, A. Borreman, and W. van Etten, "Ring resonator-based Tunable Optical Delay Line in LPCVD Waveguide Technology," *Proc. Symposium IEEE/LEOS Benelux Chapter*, (2005) pp.79-82.

[9]. A. Melloni, R. Costa, P. Monguzzi and M. Martinelli, "Ring-resonator filters in silicon oxynitride technology for dense wavelength-division multiplexing systems," *Opt. Lett*. **28**(17), (2003) pp. 1567-1569.

[10]. O. Schwelb, "Microring Resonator Based Photonic Circuits: Analysis and Design," Telecommunications in Modern Satellite, Cable and Broadcasting Services, 2007. TELSIKS 2007. 8th International Conference on, (2007) pp. 187-194.

[11]. S. Dey, S. Mandal, "Design & Analysis of Integrated Optic Filter: A Digital Signal Processing Approach," *Int. Jr. of Advanced Computer Engineering & Architecture* **2**(2), (2012) pp. 313-319.

[12]. A. Meijerink, C. G. H. Roeloffzen, L. Zhuang, D. A. I. Marpaung, R. G. Heideman, A. Borreman, W. van Etten, "," in 13th Annual Symposium on Communications and Vehicular Technology in the Benelux, IEEEE/CVT Benelux Chapter, 2006, Liège, Belgium, (2006) pp. 7-12.

[13]. L. Zhuang, C. G. H. Roeloffzen, R. G. Heideman, A. Borreman, A. Meijerink, and W.van Etten, "Single-Chip Ring Resonator-Based 1 x 8 Optical Beam Forming Network in CMOS- Compatible Waveguide Technology," *IEEE Photon. Technol. Lett*. **19**(15), (2007) pp. 1130 - 1132.

[14]. J. Verpoorte, H. Schippers, P. Jorna, C. G. H. Roeloffzen1, D. A. I. Marpaung, R. Baggen and B. Sanadgo, "Architectures for Ku-band broadband airborne satellite communication antennas," *32nd ESA Antenna Workshop on Antennas for Space Applications, 5-8 Oct 2010, Noordwijk, the Netherlands*, (2010).

[15]. S. Rabal, L. A. Bulus Rossini and P. A. Costanzo Caso, "Analysis of ORRs and its applications to implement delay lines (in Spanish)", *Proc. XV Reunión de Trabajo en Procesamiento de la Información y Control (RPIC 2013), 16- 20 Sep. 2013, Bariloche, Argentina*, (2013).

[16]. S. Granieri, M. Jaeger, and A. Siahmakoun, "Multiple-Beam Fiber-Optic Beamformer With Binary Array of Delay Lines," *J. Lightw. Technol.* **21**(12), (2003).

[17]. D. T. K. Tong and M. C.Wu, "A novel multiwavelength optically controlled phased array antenna with a programmable dispersion matrix," *IEEE Photon. Technol. Let.* **8(**6), (1996) pp. 812–814.

[18]. J. Yao, J. Yang, and Y. Liu, "Continuous True-Time-Delay Beamforming Employing a Multiwavelength Tunable Fiber Laser Source," *IEEE Photon. Technol. Let.* **14**(5) (2002) pp. 687.

[19]. B. Vidal, M. A. Piqueras, and J. Martí, "Multibeam photonic beamformer based on optical filters," *Electron. Let.* **42**(17), (2006) pp. 980–981.

[20]. P. Heimala, P. Katila, J. Aarnio, and A. Heinämäki, "Thermally Tunable Integrated Optical Ring Resonator with Poly-Si Thermistor," *J. Lightw. Technol*. **14**(10), (1996) pp. 2260-2267.

[21]. J. Cardenas, M. A. Foster, N. Sherwood-Droz, C. B. Poitras, H. L. R. Lira, B. Zhang, A. L. Gaeta, J. B. Khurgin, P. Morton, and M. Lipson, "Wide-bandwidth continuously tunable optical delay line using silicon microring resonators," *Opt. Express* **18**(25), (2010) pp. 26525-26534.

[22]. C. K. Madsen, Optical Filter Design and Analysis - A Signal Processing Approach, John Wiley & Sons, Inc. (1999).

[23]. P. A. Costanzo Caso, S. Rabal, E. Paulucci, A. Giordana, and L. A. Bulus Rossini, "Practical impairments in FBG-based true time delays," *in Latin America Optics & Photonics Conference (LAOP), 10–13 Nov. 2012 Sao Sebastiao, Brazil, 2012. Paper LM2A.21* (2012).

Caption List

Fig. 1 Scheme of tunable two-port ORR (a), and four-port ORR (b). PM: Phase modulation.

Fig. 2 (a) Response of the two ports ORR for k varying between 0.2 and 0.9, and (b) response of the four ports ORR for k_2 varying between 0.2 and 0.9 and $k_1 = 0.5$. Both figures show in the upper side the intensity transmission coefficient and in the lower side the normalized group delay for $\phi = 0$.

Fig. 3 Intensity transmission coefficient (upper side) and normalized group delay (lower side) for (a) variable phase modulation for $\phi = 0$, 0.2π, 0.4π, 0.6π and 0.8π, and (b) variable radii (or length of the ring) for 4, 5, 6, 7, and 8 mm. The variation of ϕ produces a frequency shift in the response and L modifies the FSR and the shape (peak value and FWHM) of the response. The coupling is $k = 0.5$.

Fig. 4 Cascade of three ORRs: (a) Schematic (b) Individual and resultant delays.

Fig. 5 Ring lattice composed of three ORRs.

Fig. 6 Intensity transmission coefficient and group delay for similar coupling factors, (a) and (b), and increasing coupling factors, (c) and (d).

Fig. 7 Intensity transmission coefficient and group delay for similar coupling factors, (a) and (b), and increasing coupling factors, (c) and (d).

Fig. 8 Control strategy represented in a flux diagram.

Fig. 9 Single ORR Characterization: (a) Peak value vs k, and (b) FWHM vs k.

Fig. 10 (a) Spectral separation between adjacent ORRs responses. (b) Resulting delay at the initial state. (c) Resulting delay at final state.

Fig. 11 (a) Average intensity transmission coefficient vs. average delay. (b) Coupling factors vs. average delay. (c) Ripple vs. average delay. (d) Ripple bandwidth vs. average delay.

Fig. 12 Delays implemented for each branch of the OBF system.

Fig. 13 Radiation patterns obtained for different frequencies within the ripple bandwidth for an OBF system based on (a) TTD implemented with ORRs, and (b) ideal phase shifters.

Table 1 Comparison of how parameters affect the ORR.

Figure 1.

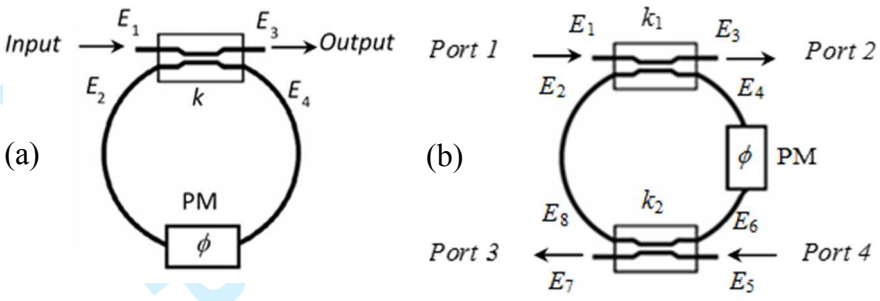

Figure 2.

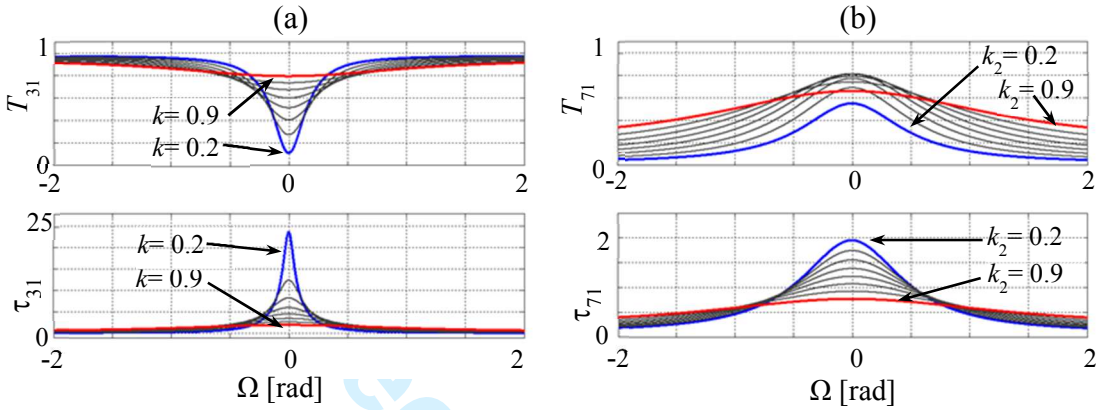

Figure 3.

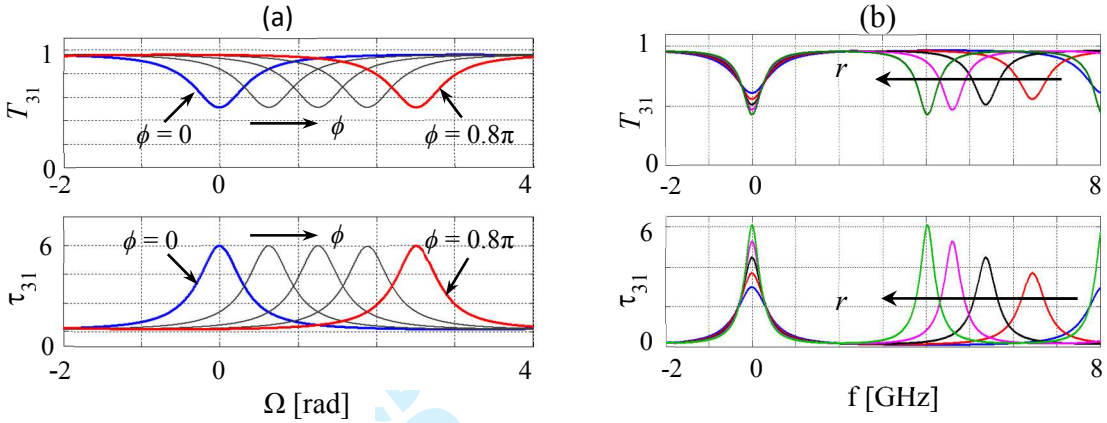

Figure 4.

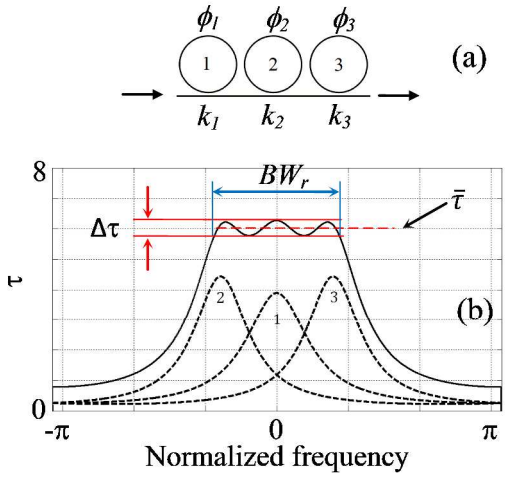

Figure 5.

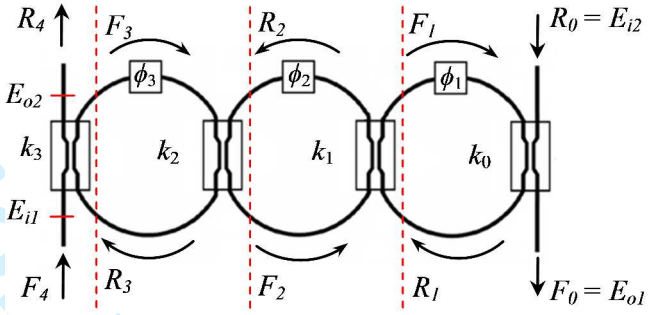

Figure 6.

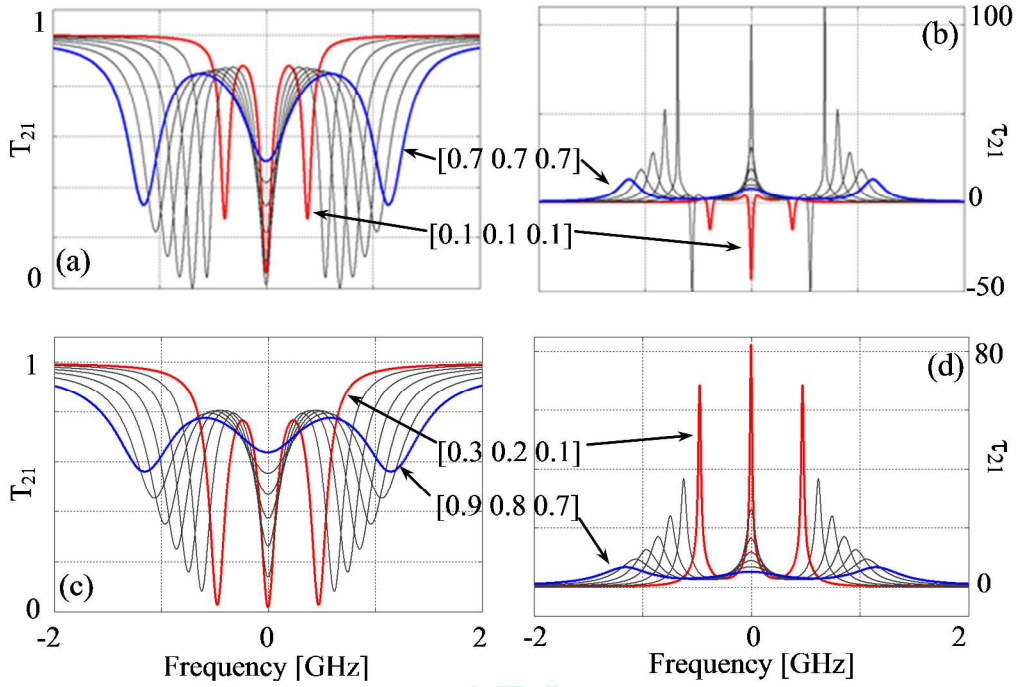

Figure 7.

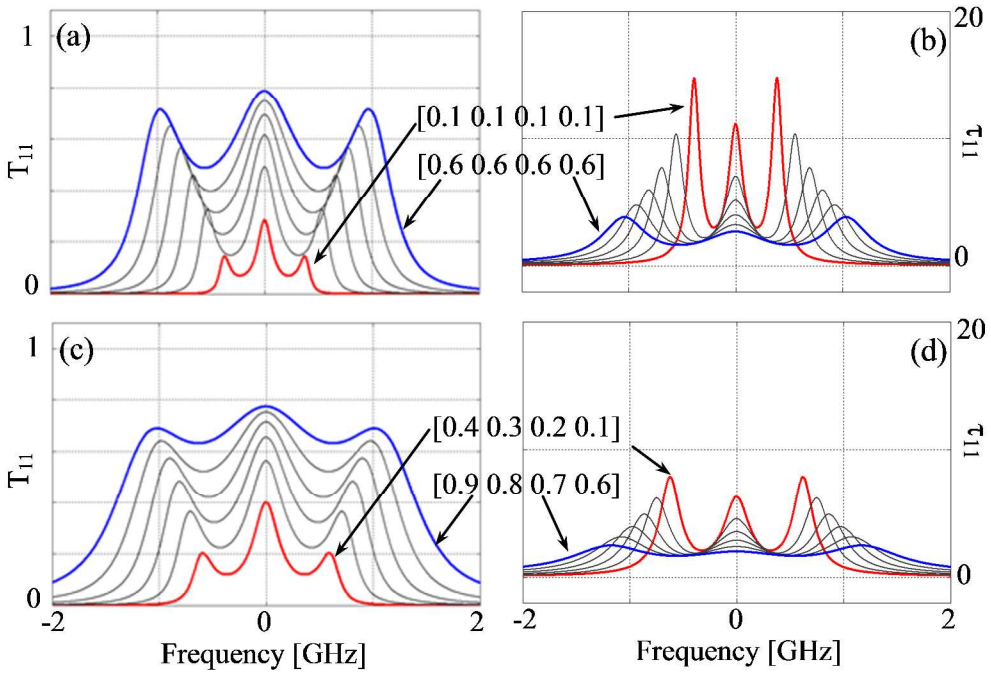

Figure 8.

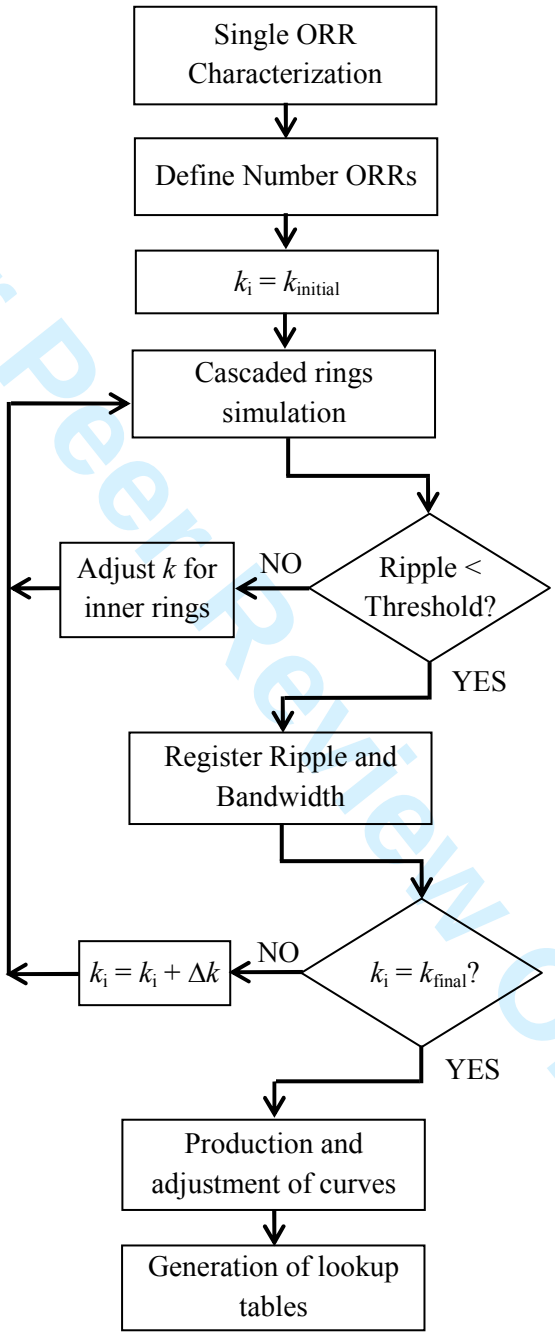

Figure 9.

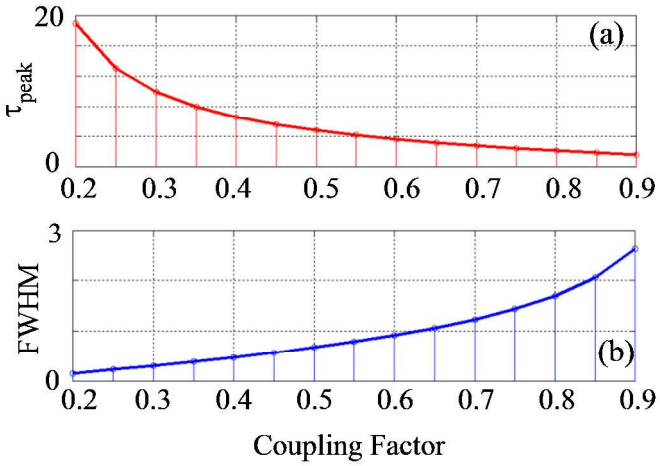

Figure 10.

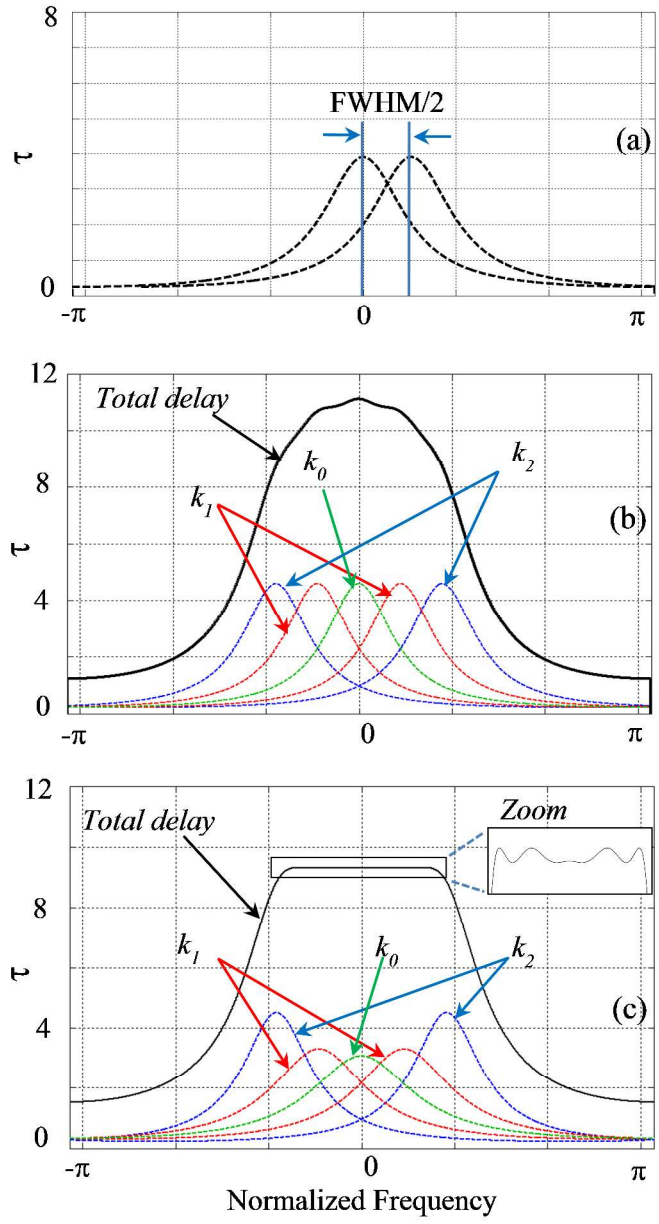
8
FWHM/2
(a)
τ
0
-π
0
π
12
Total delay
k_0
k_2
k_1
8
(b)
τ
4
0
-π
0
π
12
Total delay
Zoom
8
k_1
k_0
k_2
(c)
τ
4
0
-π
0
π
Normalized Frequency

Figure 11.

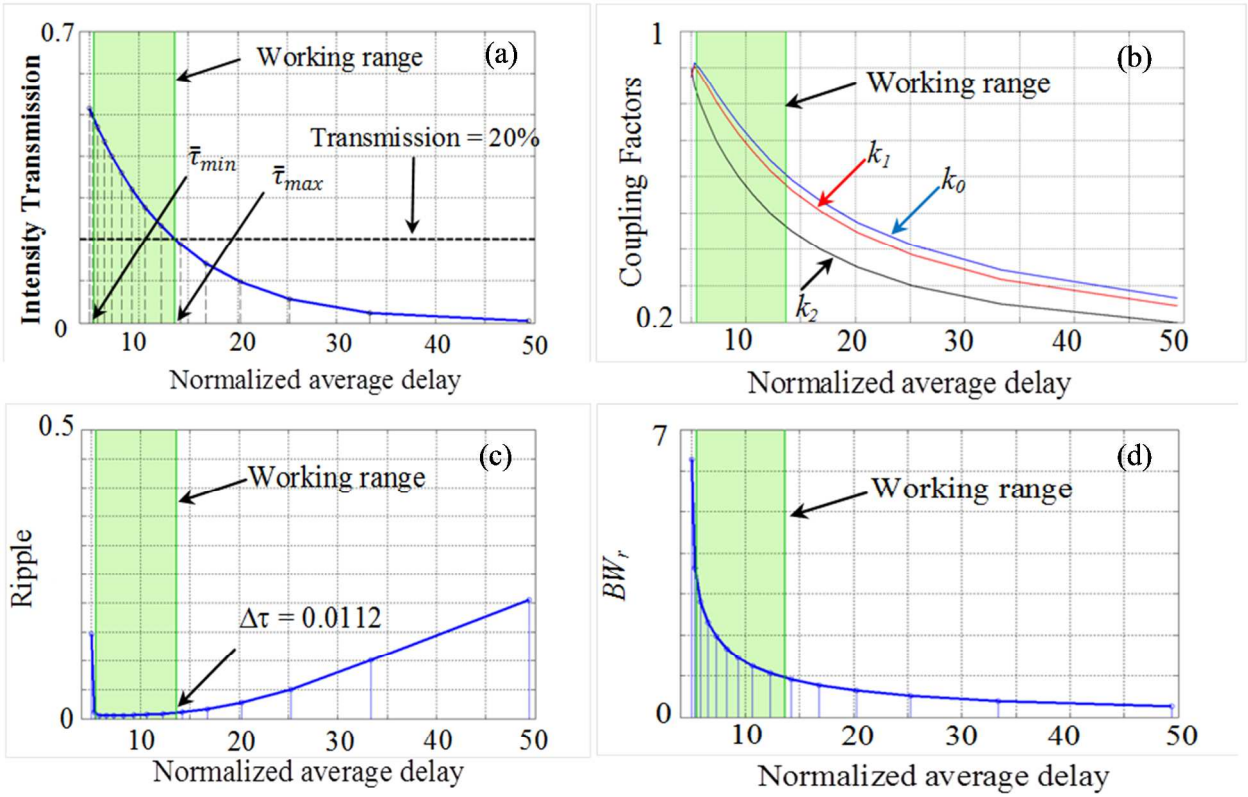

Figure 12.

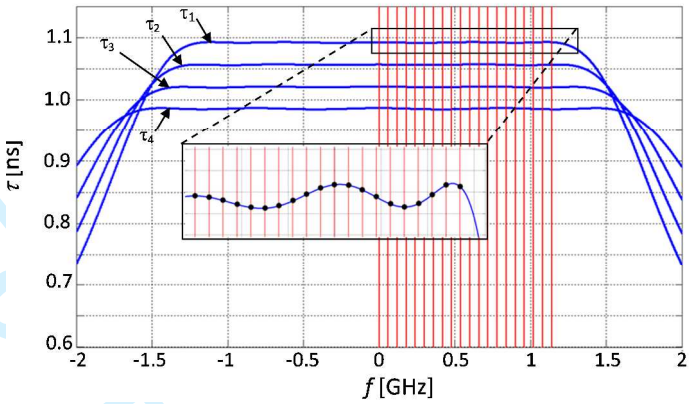

Figure 13

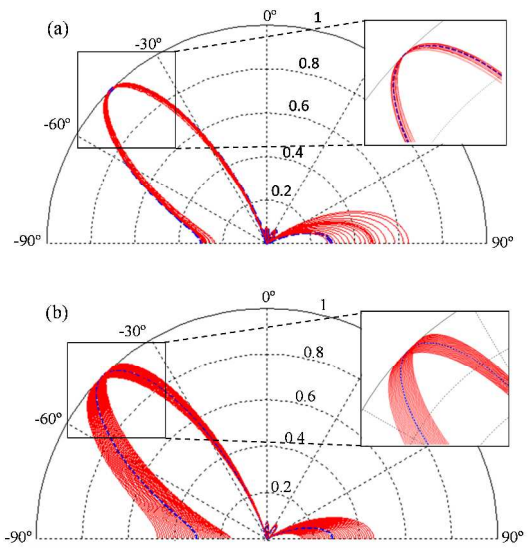

Table 1

	n_{ef}	EL	L	k	ϕ
τ peak value	Low	Low	High	High	No
FSR tunability	Low	No	High	No	No
Resonance frequency	Low	No	Medium	No	High
T variation	Low	Low	Medium	High	No
Implementation difficulty	High	Low	High	Medium	Medium